Hindawi
Shock and Vibration
Volume 2019, Article ID 5938034, 12 pages
https://doi.org/10.1155/2019/5938034

Research Article

Numerical Simulation and Experiment on Impulse Noise in a Small Caliber Rifle with Muzzle Brake

Xin Yi Zhao,[1] **Ke Dong Zhou**,[1] **Lei He**,[1] **Ye Lu**,[1] **Jia Wang**,[2] **and Qiu Zheng**[2]

[1]*School of Mechanical Engineering, Nanjing University of Science and Technology, Nanjing 201194, Jiangsu, China*
[2]*No. 208 Research Institute of China Ordnance Industries, Beijing 102202, China*

Correspondence should be addressed to Ke Dong Zhou; zkd81151@njust.edu.cn and Lei He; hlhlhxh@njust.edu.cn

Received 29 June 2019; Revised 31 July 2019; Accepted 10 August 2019; Published 9 September 2019

Academic Editor: Giuseppe Ruta

Blast waves generated from the muzzles of weapons may exert negative effects, such as shock waves and impulse noise. If the weapon is fired with a muzzle brake, these effects are recognized to be more severe. This paper discusses the influence of the muzzle brake on certain aeroacoustic noise characteristics based on numerical simulations and a corresponding experiment. The impulse noise, which is induced by complex jet flows discharging from small caliber rifles with muzzle brakes, is focused in this study. Computational fluid dynamics (CFD) and computational aeroacoustics (CAA) are combined to calculate the muzzle flow field and jet noise for cases with and without a muzzle brake, and then the data sets are carefully compared. The simulations indicate that the muzzle brake alters the muzzle flow field and directional distribution of the jet noise compared to a rifle sans muzzle brake. Deviations less than 7.6% between experimental data and simulation results validate the simulation model. The results presented in this paper may provide a workable reference for the prediction of muzzle noise and the optimization of muzzle brake designs.

1. Introduction

The use of muzzle brakes represents an important innovation in combat systems as they force the forward momentum of muzzle gases rearward to offset the recoil load created by the weapons during firing. Redirecting the muzzle gases also increases the intensity of the shock wave, however, as well as the impulse noise behind the guns. These factors have various negative effects on human bodies and environments.

Early research on muzzle flow [1–9] and classical theories seldom involve the calculation and prediction of the muzzle noise field under muzzle brake conditions due to the complex structure of both the muzzle device and flow field itself. Experiments do not reveal changes in the flow field caused by the muzzle brake, nor do they fully reflect the development and propagation of the muzzle noise field. Furthermore, weapon testing in both near and far flow fields is very expensive as it requires a great deal of manpower and resources. Numerical calculations can simulate the flow field near the muzzle via computational fluid dynamics (CFD) and simply calculate the noise [10, 11] but are not suitable for muzzle noise in far fields as the computational aeroacoustics (CAA) has an oversize computational domain and stringent precision requirements.

Advancements in computational performance and CAA have made numerical simulation methods better suited to jet noise research [12–20]. The muzzle noise production and development mechanism has also been researched using CFD-CAA hybrid methods [21–24]. However, researchers tend to investigate muzzle noise without any muzzle devices; there have been few previous studies of muzzle noise taking the muzzle brake into account.

Preliminary research on muzzle jet flow noise based on both simulation and experimental data was conducted in this study to analyze the effects of the muzzle brake on the intensity and directivity of muzzle noise. A 5.8 mm caliber automatic rifle with a standard 5.8 mm cartridge was selected as the research object. A CFD-CAA hybrid method was used to calculate the muzzle flow field by the large eddy simulation (LES) method, and the noise attenuation was determined by using Ffowcs Williams and Hawkings (FW-H)

equations based on the obtained source data. The jet noise induced by complex flows discharging from the rifle was analyzed. The effect of the muzzle brake on noise propagation characteristics is discussed below by comparison of the results with and without a muzzle brake. The simulation results were also compared against experimental data to validate the model. The results presented here may provide a useful reference for predicting the muzzle noise and optimizing muzzle brakes for small caliber weapon systems.

2. Methodologies

2.1. Muzzle Noise Characteristics. Due to the supersonic speed at which propellant gas exhausts from the gun barrel, an unsteady flow field with high temperature, high pressure, and high speed is formed around the muzzle as shown in Figure 1. The flow field is very complex; it includes the muzzle shock waves (initial shock wave and propellant gas shock wave), impulse noise wave, and high-temperature propellant gas flow. Pressure perturbations throughout the muzzle flow field together comprise the source of muzzle noise [6].

Muzzle noise has two main sources. The first is shock wave noise, which is mainly formed by the decay of muzzle shock wave below 6.9 kPa (170.7 dB) [6]. The essence of shock wave noise is still weak shock waves. The second source is impulsive noise caused by factors such as turbulent fluctuation in the mixing zone of the expanded jet at high speeds or the unstable shock wave in muzzle flow; its essence is the radiation noise. Most of this kind of noise attenuates and disappears in the early stage of muzzle flow field formation. Generally speaking, the main impulse noise in the muzzle system is generated by the propelled gas turbulent jet [20, 21]. To calculate shock wave noise, it is necessary to obtain pressure perturbations at the measuring points by directly solving compressible the Navier–Stokes equations, this requires a wide computational domain with a large quantity of grids that are beyond existing computational conditions. The radiated noise can be calculated by CFD-CAA hybrid methods, as discussed in detail below.

There are differences between the two kinds of muzzle noise in terms of sound source properties and calculation methods. They needed to be studied separately. Therefore, this research only focuses on impulse noise. During the simulation, a supersonic projectile of a rigid body was not considered as the impact of the projectile, and initial shock wave (produced as compressed air from a supersonic moving projectile exiting the barrel) on muzzle noise is very small compared to the two factors discussed above [6, 20].

2.2. Governing Equation. The CFD-CAA hybrid method provides the flexibility to select the most appropriate method for each problem. For simulating the sound source fields, the hybrid method utilizes flow solvers of CFD, such as direct numerical simulation (DNS) or large eddy simulation (LES). The far field sound is computed with CAA methods, such as the FW-H acoustic analogy method or extended Kirchhoff method. In this study, the LES method was used to compute the flow field and the propagation of acoustic waves in the far field was determined by solving the FW-H integration equations. Both methods are described in detail in the following sections.

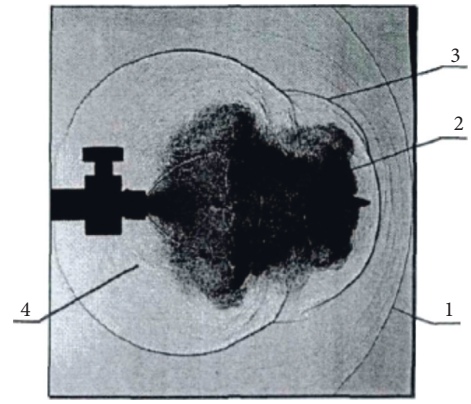

Figure 1: High-speed shadow photo of muzzle flow field, 7.62 mm ballistic gun. 1: initial shock wave; 2: propellant gas flow; 3: propellant gas shock wave; 4: impulsive noise wave.

2.2.1. LES Method. The LES method is considered to be a suitable CFD approach to simulate a turbulent flow with high Reynolds number. The basic principle of the LES is to provide an alternative weighted average of the N-S equation in space. The large-scale and small-scale turbulent structures are calculated separately by a spatial filtering method. Eddies smaller than a preset scale are filtered out from the flow field and obtained by solving additional equations. Only the large eddies are calculated time-dependently. The continuity equation and N-S equation after filtering can be expressed as

$$\frac{\partial \rho}{\partial t} + \frac{\partial}{\partial x_i}\left(\rho \overline{u_i}\right) = 0,$$
$$\frac{\partial}{\partial t}\left(\rho \overline{u_i}\right) + \frac{\partial}{\partial x_j}\left(\rho \overline{u_i}\,\overline{u_j}\right) = \frac{\partial}{\partial x_j}\left(\mu \frac{\partial \sigma_{ij}}{\partial x_j}\right) - \frac{\partial \overline{p}}{\partial x_i} - \frac{\partial \tau_{ij}}{\partial x_j}, \tag{1}$$

where $\overline{u}_i$ denotes the average velocity component after filtering, σ_{ij} is the stress tensor due to molecular viscosity, and τ_{ij} is the subgrid-scale stress. They are defined as follows:

$$\sigma_{ij} = \left[\mu\left(\frac{\partial \overline{u_i}}{\partial x_j} + \frac{\partial \overline{u_j}}{\partial x_i}\right)\right] - \frac{2}{3}\mu \frac{\partial \overline{u_i}}{\partial x_i}\delta_{ij},$$
$$\tau_{ij} = \rho \overline{u_i u_j} - \rho \overline{u_i}\,\overline{u_j}, \tag{2}$$

where δ_{ij} is a Kronecker function. In this paper, a Smagorinsky–Lilly model is used to simulate sublattice stress. Detailed model descriptions are available in reference [25].

2.2.2. FW-H Acoustic Analogy Method. Ffowcs Williams and Hawkings utilized the generalized function theory to obtain the classic equation associated with their names. According to the continuous equation and momentum equation, the FW-H equation is

$$\frac{1}{c_0^2}\frac{\partial^2 p'}{\partial t^2} - \nabla^2 p' = \frac{\partial^2}{\partial x_i \partial x_j}\left[T_{ij}H(f)\right] - \frac{\partial}{\partial x_i} \cdot \left\{\left[P_{ij}n_j + \rho u_i\left(u_n - v_n\right)\right]\delta(f)\right\} + \frac{\partial}{\partial t}\left\{\left[\rho_o v_n + \rho\left(u_n - v_n\right)\right]\delta(f)\right\}, \quad (3)$$

$$H(f) = \begin{cases} 0, & f = 0, \\ 1, & \text{elsewhere}, \end{cases}$$

$$\delta(f) = \frac{d}{df}\left[H(f)\right],$$

where p' is the fluid pressure used in the acoustic field and c_0 is the sound velocity, T_{ij} is the Lighthill stress tensor, P_{ij} is the compressible fluid stress tensor, u_n is the fluid velocity component normal to the surface $f = 0$, v_n is the surface velocity component normal to the surface, $H(f)$ is the Heaviside function, and $\delta(f)$ is the Dirac delta function.

The three terms on the right-hand side of the FW-H equation represent the acoustic radiation source: the first term indicates the turbulent stress of the fluid itself with quadrupole characteristics, the second one represents the dispersion of the unstable forces applied to some interfaces with dipole characteristics, and the third one indicates the unsteady mass flowing into the fluid with monopole characteristics.

2.3. Evaluation Parameters of Noise. Sound pressure level (SPL) is a basic measurement for the pressure fluctuations of a sound wave as it propagates through the air [26]:

$$\mathrm{SPL} = 20\lg\frac{p'}{p_{\mathrm{ref}}}, \quad (4)$$

where p' is the perturbation pressure calculated by subtracting the mean pressure and p_{ref} is the reference sound pressure, which is usually equal to the minimum human auditory threshold, $p_{\mathrm{ref}} = 2 \times 10^{-5}$ Pa.

The SPL for the weapon muzzle noise is mostly determined by peak sound pressure level ($\mathrm{SPL}_{\mathrm{peak}}$) and overall sound pressure level (OASPL) [27]. $\mathrm{SPL}_{\mathrm{peak}}$ is the SPL corresponding to the peak value of pressure-time curve, while OASPL is the accumulated result of all frequencies:

$$\mathrm{SPL}_{\mathrm{peak}} = 20\lg\frac{p_{\mathrm{peak}}}{p_{\mathrm{ref}}}, \qquad \mathrm{OASPL} = 10\lg\left(\sum_i 10^{\mathrm{SPL}_i/10}\right), \quad (5)$$

where SPL_i is the sound wave pressure level from the ith harmonic wave.

3. Experiment

3.1. Experimental Scheme and Setup. The experiment was conducted in a semisilencing room, with an effective space of 9.32 m × 7.84 m × 5.26 m at the No. 208 Research Institute of China Ordnance Industries. The room has five surfaces equipped with sound-absorbing material (the ground is not) with effective sound insulation and vibration isolation performance. A 5.8 mm caliber automatic rifle was selected as the research object in this study. The muzzle brake of the rifle used in these tests is shown in Figure 2.

The test system mainly consists of acoustic sensors and an acquisition control system as shown in Figure 3; Figure 4 shows a photo of the experimental setup. The acoustic sensors are G.R.A.S type 46BE quarter-inch free field microphones without the foam windscreen. The microphones were connected to the acquisition control system, Siemens LMS SC310-UTP. The axis of the microphone was set vertical to the ground, and each microphone was mounted on a weighted tripod. The height of the tripod was adjusted to make sure that the microphone was in level with the gun barrel axis throughout the experiment, approximately 1 m above the ground level. The microphone signal was recorded by using LMS SC310-UTP with 102400 Hz sampling frequency and the sampling time of 5 s. The data of individual shots were analyzed in LMS Test.Lab software.

Sound levels were measured with radii of 1.0 m, 1.5 m, 2.0 m, and 2.5 m at 0°, 45°, and 90° counterclockwise from the downstream direction of the jet. An overview of the measurement points and the corresponding field diagram are shown in Figures 5 and 6, respectively. The shooter fired one round at a time, not in bursts, and ten single rounds were recorded at each point. The microphone calibration was checked before each test using a B & K 4231 sound level calibrator.

3.2. Experimental Result Analysis. The same behavior was observed in all ten rounds of the experiment, so the result from the sixth round was taken as an example for further analysis. The pressure varies with time at different measurement points and their corresponding one-third octave frequency spectra are shown in Figure 7.

As described in Section 2.1, the muzzle flow field is very complex and contains both shock waves and noise waves. The experimental data obtained from various measurement points reflect not only the nonlinear flow phenomenon of shock waves but also a series of impulse noise waves (Figures 7(a)–7(c)). The spectra corresponding to the curves of pressure-time at each measurement point are shown in Figures 7(d)–7(f). It appears that muzzle noise is a broadband continuous spectrum with obvious peak frequency and high sound energy in each band. The spectrum shape markedly differs at different angles.

This study focuses on the impulse noise; therefore, the shock wave noise has been filtered before calculating the OASPL at each point for comparison against the simulation results. According to the characteristics of the muzzle flow field, the initial shock wave and muzzle blast wave formed prior to gas jet propulsion and have a higher propagation speed. The shock wave can thus be excluded from the analysis by the first period of the measurements in the *P-T* curve. For example, at point 1 the period before 3.292 s has

Figure 2: Experimental rifle with the muzzle brake.

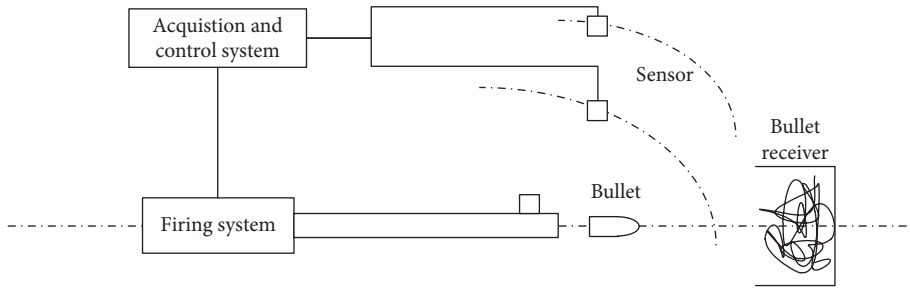

Figure 3: Schematic diagram of the test scheme.

Figure 4: Experimental setup.

Figure 6: Field diagram (red line indicates the axis of different angles according to barrel axis; red circle indicates microphone location).

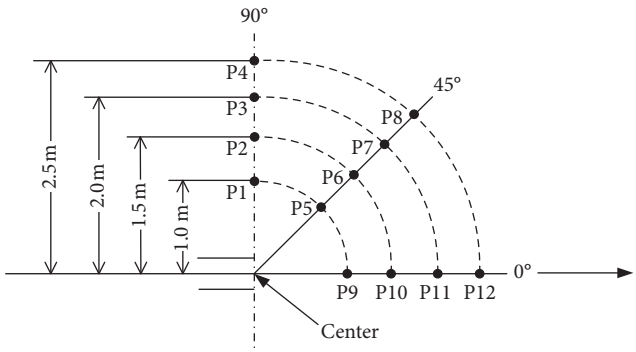

Figure 5: Measurement point locations in the far field.

been excluded from the calculation of impulse noise (Figure 7(a)). The average SPL_{peak} and OASPL of the impulse noise for 10 rounds at all the measurement points are shown in Table 1.

As described in reference [27], one of the primary characteristics of muzzle noise is a typical difference between SPL_{peak} and OASPL. The value of this difference varies with the type of weapon and shooting environment; it is generally between 15 and 30 dB. As shown in Table 1, the difference of the testing weapon in this study is between 23.5 and 29 dB. The values at $\theta = 0^{\circ}$ and $\theta = 90^{\circ}$ are higher with the majority

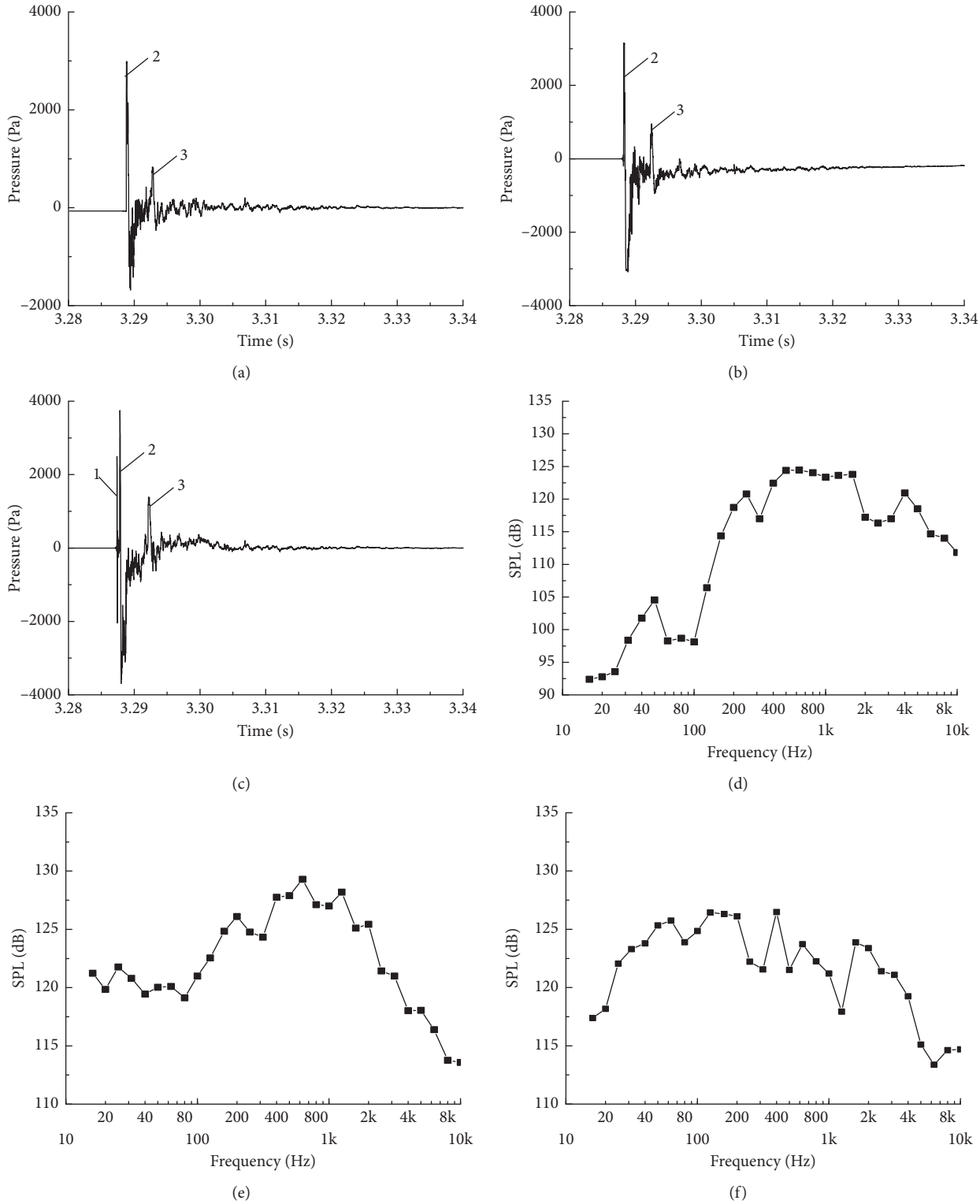

Figure 7: Sound pressure level varying with time and the corresponding one-third octave frequency spectrum at different measurement points. (a) *P-T* at point 1. (b) *P-T* at point 5. (c) *P-T* at point 9. (d) SPL-*f* at point 1. (e) SPL-*f* at point 5. (f) SPL-*f* at point 9. 1: initial shock wave; 2: muzzle blast; 3: impulse noise wave.

laying in the range of 26–28 dB; the typical value is 27 dB. For the points at $\theta = 45^{\circ}$, there are less differences as the values are around 23.5–24.5 dB with a typical value of 24 dB. The noise components in the jet fluid direction ($\theta = 0^{\circ}$) and side hole position ($\theta = 90^{\circ}$) are more complex and lead to relatively greater differences.

Table 1: Average measured SPL_{peak} and OASPL of impulse noise.

	SPL_{peak} (dB)	OASPL (dB)	Difference (dB)
Point $\theta = 90^\circ$			
P1	152.38	126.26	26.12
P2	151.21	124.83	26.38
P3	150.44	123.34	27.10
P4	150.35	121.82	28.53
Point $\theta = 45^\circ$			
P5	156.08	131.73	24.35
P6	153.9	130.18	23.72
P7	152.54	128.65	23.89
P8	150.21	125.6	24.61
Point $\theta = 0^\circ$			
P9	161.63	132.77	28.86
P10	159.85	131.01	28.84
P11	157.38	130.08	27.30
P12	156.11	129.2	26.91

4. Numerical Simulation

4.1. Small Caliber Rifle with Muzzle Brake. The muzzle brake used in the experiment was schematized in a 3D physical model as shown in Figure 8. Considering the circumferential symmetry of the muzzle brake, 1/6 of the model was used for numerical simulation to describe the problem sufficiently with a minimal number of grids and enhanced the computational efficiency. A schematic diagram of the computational domain scaled down by the muzzle diameter (d) is shown in Figure 9. The length of the exterior flow field was set to 115 times of the diameter (~95d in the downstream direction and ~20d in the upstream direction), and the radial size was about 45d. The whole structure mesh was divided by the hybrid grid method. The unstructured grids were applied to the complex muzzle brake, and the rest were schematized as hexagonal grids. The grid spacing in this case is nonuniform and the total grid number is 2,720,810 (Figure 10). The mesh size has been determined by evaluating the influence of the grid on the model outcome. The density of the mesh utilized shows similar results as a more refined grid, at a third of the calculation time of the refined grid.

As the initial shock wave and the projectile were not taken into consideration in this study, the start time of the muzzle flow field calculation was determined as the moment when the projectile leaves the muzzle and the propellant gas begins to flow outward (i.e., the end of the interior ballistics). The initial conditions such as pressure and velocity in the barrel were determined by using the internal ballistics equations below as shown in Figure 11:

$$u_x = \frac{v}{L}x,$$
$$p_x = p_d\left[1 + \frac{m_p}{2\varphi_1 m}\left(1 - \frac{x^2}{L^2}\right)\right], \quad (6)$$

where u_x is the velocity of the propellant gas, v is the velocity of the projectile, L is the length of the chamber, p_x is the pressure of the propellant gas, p_d is the pressure at the bottom of the projectile, m_p is the charge quantity, m is the projectile mass, and φ_1 is the secondary work coefficient.

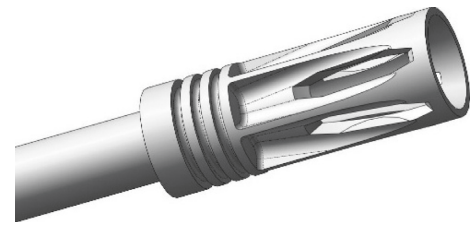

Figure 8: Schematic diagram of the muzzle brake.

An average temperature of 1800 K was used as the initial temperature in the chamber, and the atmosphere of the region out of the chamber was set to 101,325 Pa and 300 K. All the initial conditions are set through the user-defined function (UDF) program according to ANSYS FLUENT 15.0 UDF Manual.

The outer surfaces of the barrel and muzzle brake were specified as a wall boundary (Figure 9). The domain boundary around the muzzle flow field was specified as the pressure-outlet boundary.

4.2. Small Caliber Rifle without Muzzle Brake. To investigate the muzzle noise field with the muzzle brake, the same weapon with no muzzle brake was built for the sake of comparison. A schematic diagram of its computational domain, initial conditions, and boundary conditions is shown in Figure 12. Everything except for the muzzle brake and the scale of the computational domain is identical to the previous case. The length of exterior flow field was set to 150 times the diameter (~130d in the downstream direction and ~20d in the upstream direction) which is longer than the other case as the propellant gas is stronger in the jet flow direction. The whole structure mesh was divided by the hexagonal grid, and the total grid number is 2,501,860.

4.3. Solution Method. According to the CFD-CAA hybrid method, there are two steps in the analysis of aerodynamic noise. First, all computational domains are analyzed by the LES method. Here, unsteady flow parameters such as destiny, pressure, and velocity were collected on the source surface after obtaining stable unsteady solution during 10,000 time steps for a total time exploration of 50 ms. The sound propagation was computed by using the FW-H equation to obtain the sound pressure signal of each receiver. All calculations were completed in ANSYS-FLUENT software.

The location of the FW-H surface used as necessary inputs for acoustic calculations in the far fields is shown in Figures 9 and 12. The distribution of sound receivers is shown in Figure 13. The muzzle noise field was monitored with the radii of 0.5 m, 1.0 m, 1.5 m, 2.0 m, and 2.5 m every 10° counterclockwise from the downstream direction of the jet. Receivers at 45° were also set corresponding to the experimental points. To ensure an appropriate comparison regarding the influence of the muzzle brake on sound pressure level in the ambient region, the points of all receivers were given the same distances and angles for both cases.

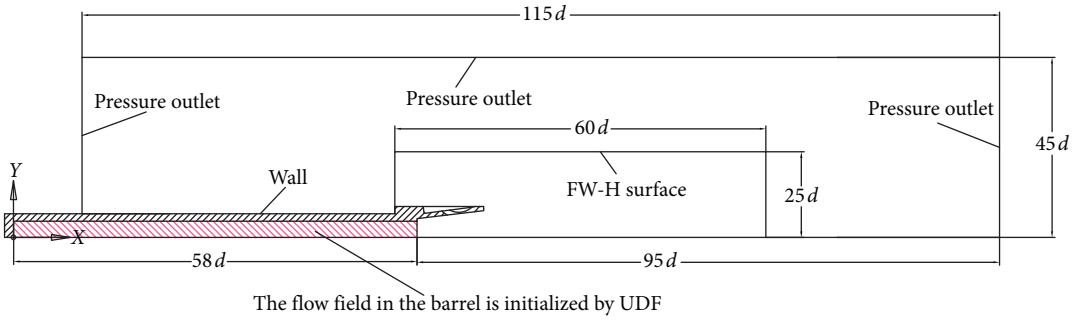

Figure 9: Schematic diagram of the computational domain and boundary condition.

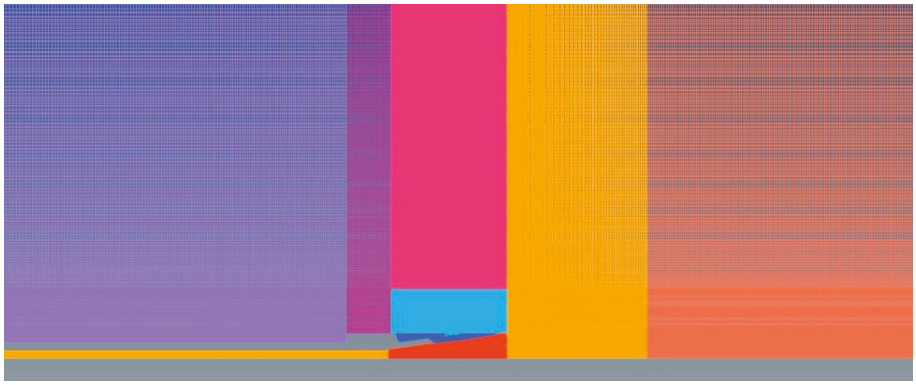

Figure 10: Grid model of the computational domain.

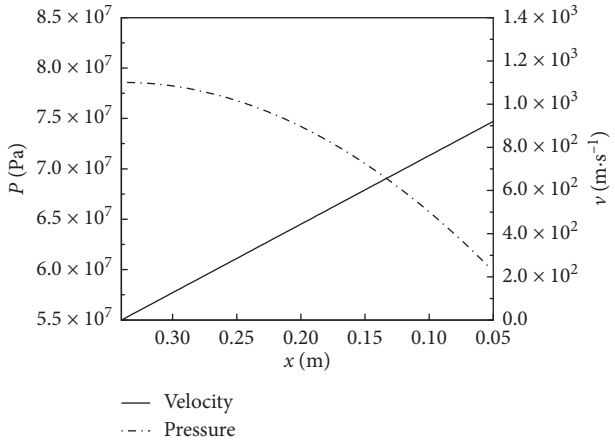

Figure 11: Initial condition.

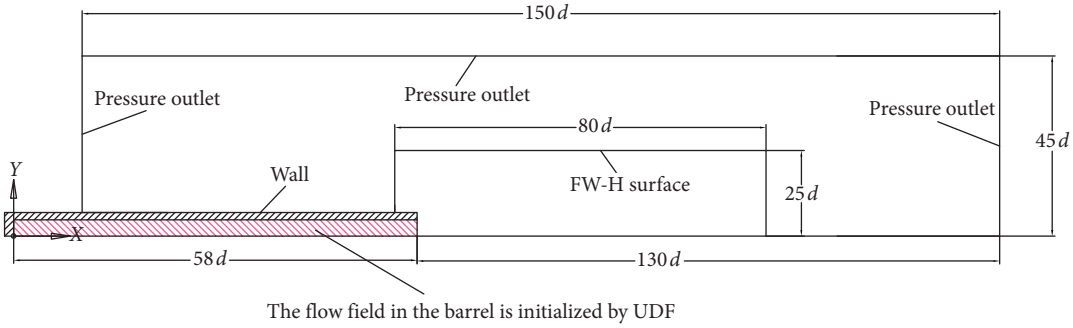

Figure 12: Schematic diagram of the computational domain and boundary condition.

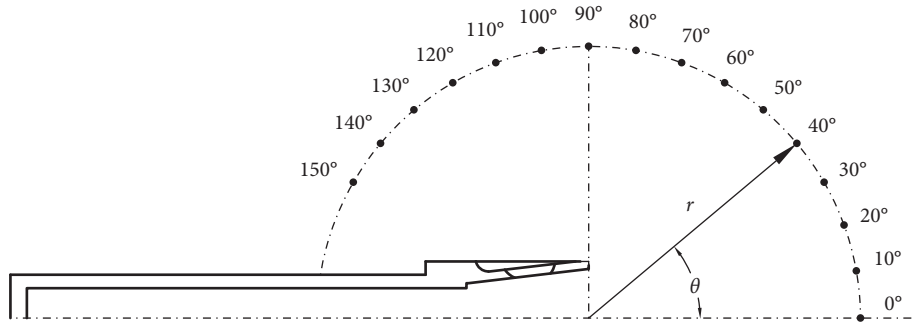

Figure 13: Receiver locations in the far field.

5. Results and Analysis

5.1. Analysis of the Case with Muzzle Brake. Jet flow from the muzzle is instantaneous, high-pressure, and inconstant as shown in Figure 14.

When the CFD calculation is relatively stable, the FW-H equation is applicable to calculate the sound pressure of each receiver location based on the source data obtained from the numerical LES results. The OASPL can then be determined by spectral analysis. A corresponding noise directivity diagram is shown in Figure 15.

For the receivers located at the radius equal to 0.5 m, which are nearest to the muzzle, the maximum OASPL value is 136.5 dB at 50°. As the radius increases, the angle of the maximum value gradually falls to the side. The maximum values of all the rest of the receivers are reached at 90°. One of the reasons for this difference is that turbulent jet noise is the most common quadrupole noise and has obvious directivity, which reaches its maximum value at about 45° [26]. The receivers at $r = 0.5$ m are in the near field close to the muzzle, i.e., within the jet cone range. They are affected by the quadrupole noise source and show similar directivity. However, when the radius increases, they are less affected by the quadrupole noise source in the jet cone when farther away from this region.

The characteristics of noise are also closely related to the structure of muzzle flow field. Previous research [27] has shown that the muzzle noise of weapons without muzzle devices has strong directivity with most acoustic energy concentrated in ±75°. The sound pressure level at 90° is approximately equal to the average sound pressure level in the circumference. The presence of the muzzle brake results in the propellant gas escaping through side hole and enhancing the flow at large azimuth angles. Therefore, for receivers far away from muzzle, the maximum value emerges at 90°.

5.2. Comparison of the Cases with and without Muzzle Brake. A comparison of the simulated results at different angles and radii for cases with and without a muzzle brake is shown in Figure 16. As shown in Figure 16(a), the angle at which the maximum value is reached changes from 60° without the muzzle brake to 90° with the muzzle brake. A similar phenomenon can be observed with receivers on other radius positions in Figure 16(b). Installation of the muzzle brake appears to have little effect on the noise downrange ($\theta = 0$–$70°$) but increases the sound pressure level on the side and the rear of the muzzle ($\theta = 70$–$150°$).

5.3. Comparison of Modeled and Experimental Results. The simulated and experimental results were compared based on the peak frequency and peak sound pressure level to verify the accuracy and feasibility of the model.

5.3.1. Peak Frequency. Peak frequency is an important part of spectrum analysis and also the basis for noise source analysis. The spectra of points at different angles are shown in Figure 17. As shown in Figure 17(a), the peak frequency of turbulent noise obtained by numerical simulation is 4 kHz, which is in the 4k center frequency range of the one-third octave frequency spectrum. The same pattern is visible in Figures 17(b) and 17(c). It appears that turbulent noise is one of the reasons for the peak frequency in the muzzle noise spectrum; impulsive noise caused by the propellant gas turbulent jet is one of the main sources of muzzle noise.

5.3.2. Peak Sound Pressure Level. The SPL_{peak} is commonly used as global standards for noise from weapons. The simulated data were further processed by combining the OASPL and typical difference value obtained from measured data to estimate SPL_{peak}. A comparison of SPL_{peak} values for different methods is shown in Table 2.

The simulated results of the points at $\theta = 90°$ and $\theta = 45°$ match the experimental data well with deviation less than 2.5% and 5.5% repetitively. However, for the points at $\theta = 0°$, the model shows relatively larger discrepancy from the experiment. A difference of 7.6% emerged at point 12. The data measured from the experiment include initial jet flow noise, propellant gas jet flow noise, and a sonic boom due to the supersonic projectile. The sonic boom and initial jet flow noise are beyond the scope of this study because the projectile moving body was not considered; therefore, deviations are to be expected. The resolution of the model also has a limited prediction frequency of sound source; the solution is unable to cover the high-frequency sound source thus causing some discrepancy to this effect.

Based on Table 2, the deviation of estimated SPL_{peak} of impulse noise from measured data is within 7.6%. For the points at $\theta = 90°$, the difference is lower than 2.5%. These

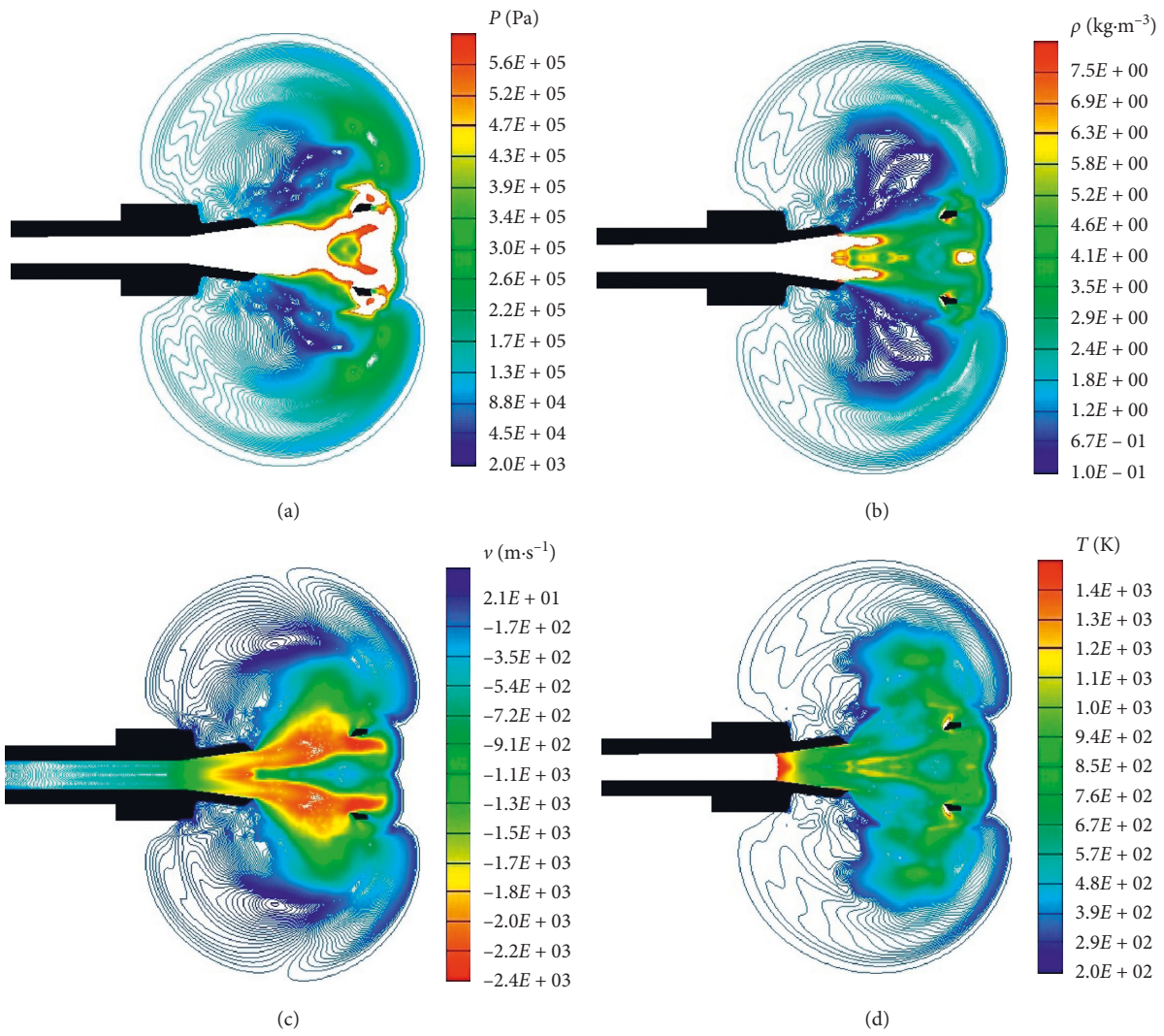

Figure 14: Muzzle flow field at $t = 0.5$ ms. (a) Pressure contours. (b) Density contours. (c) Velocity contours. (d) Temperature contours.

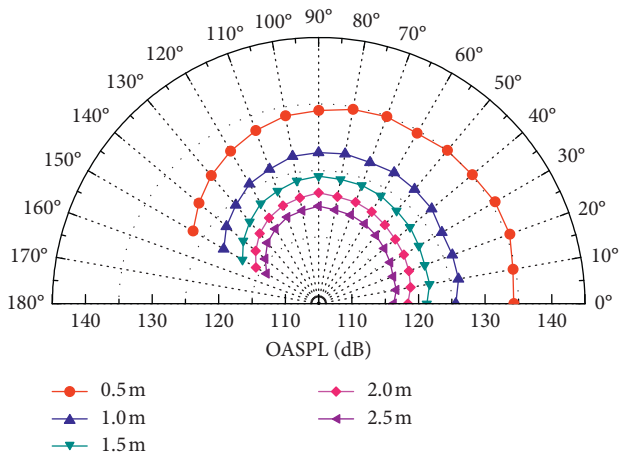

Figure 15: Noise directivity diagram.

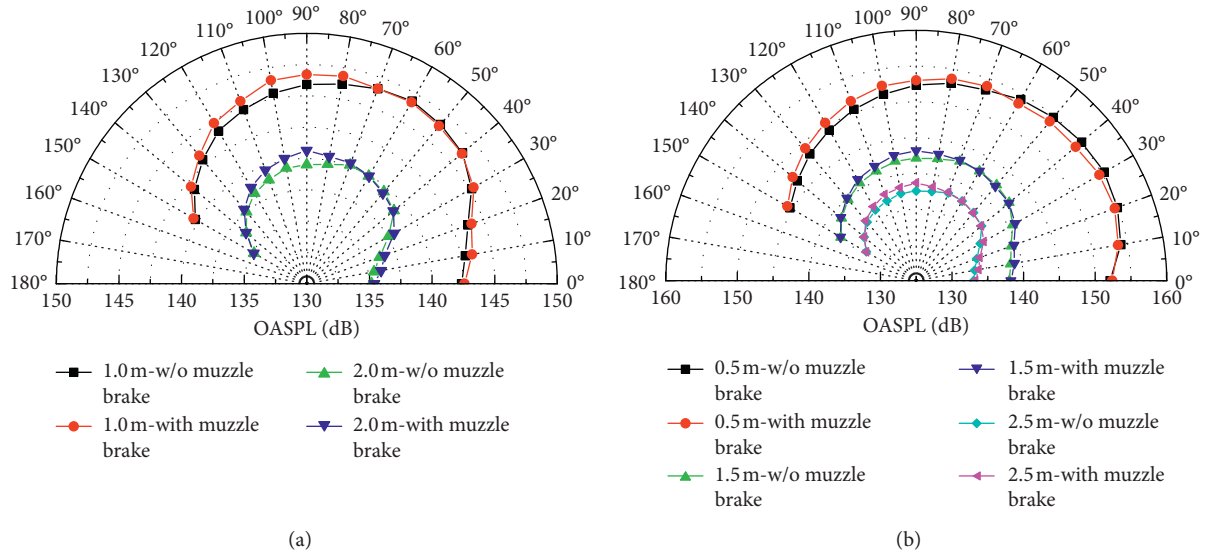

(a) (b)

Figure 16: Noise directivity diagrams with and without the muzzle brake. (a) $r = 1.0$ and 2.0 m. (b) $r = 0.5$ m, 1.5 m, and 2.5 m.

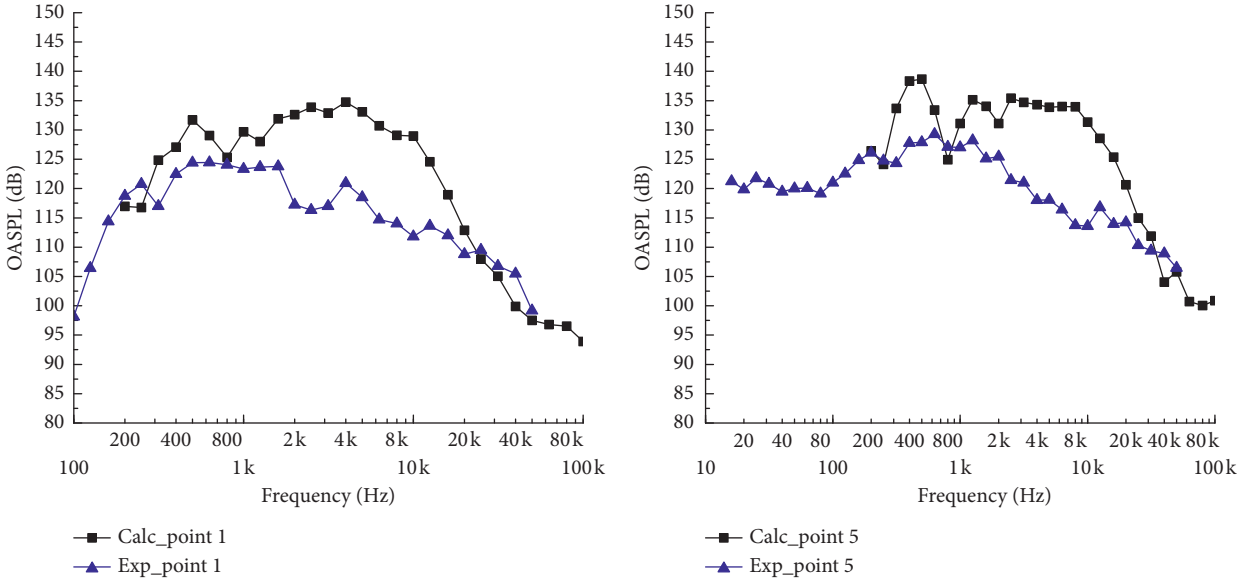

(a) (b)

Figure 17: Continued.

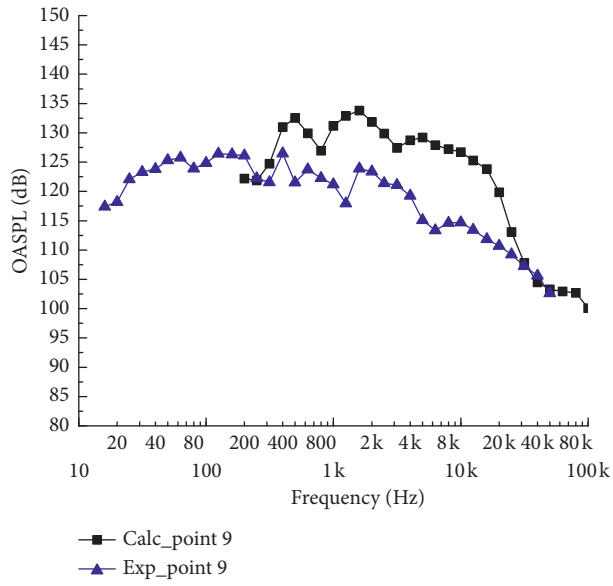

(c)

Figure 17: One-third octave frequency spectrum. Comparison between cases with and without the muzzle brake. (a) Point 1 at $\theta = 90^{\circ}$ and $r = 1.0$ m. (b) Point 5 at $\theta = 45^{\circ}$ and $r = 1.0$ m. (c) Point 9 at $\theta = 0^{\circ}$ and $r = 1.0$ m.

Table 2: Comparison between the calculated and experimental results of SPL_{peak}.

	SPL_{peak} (dB)		Difference (%)
	Measured	Calculated	
Point $\theta = 90^{\circ}$			
P1	152.38	154.69	−1.5
P2	151.21	151.16	0.0
P3	150.44	148.65	1.2
P4	150.35	146.67	2.4
Point $\theta = 45^{\circ}$			
P5	156.08	151.26	3.1
P6	153.9	147.22	4.3
P7	152.54	145.42	4.7
P8	150.21	142.35	5.2
Point $\theta = 0^{\circ}$			
P9	161.63	153.59	5.0
P10	159.85	149.24	6.6
P11	157.38	146.4	7.0
P12	156.21	144.26	7.6

results suggest that the simulation can indeed feasibly replicate reality.

6. Conclusions

A CFD-CAA hybrid method was used in this study to simulate the impulse noise from a small caliber rifle with/without a muzzle brake. The model was validated by comparison with experimental data. The conclusions can be summarized as follows:

(1) In the case with a muzzle brake, the clear directivity of quadrupole noise can be observed within 0.5 m away from the muzzle's central point. The directivity grows less intensely as the radius increases, and the peak emerges at $\theta = 90^{\circ}$ for the calculation points farther than 1.0 m. For the case without a muzzle brake, the results differ. It suggests that the muzzle brake alters the construction of the flow field, thus influencing sound-field propagation.

(2) Comparison of the peak frequency between the simulated and experimental results indicates that the impulse noise caused by the propellant gas jet flow is one of the main sources of muzzle noise.

(3) The deviation between simulated results and experimental data is within 7.6%, which indicates that the proposed simulation method is feasible.

The research presented in this paper may be helpful as future engineers seek to better understand impulse noise characteristics; they may also provide a workable reference for designing muzzle brakes for small caliber weapon systems.

Data Availability

All data included in this study are available from the corresponding author upon request.

Conflicts of Interest

The authors declare that there are no conflicts of interest regarding the publication of this paper.

Acknowledgments

This work was supported by the Natural Science Foundation of China (Grant No. 11802138).

References

[1] J. I. Erdos and P. D. Del Guidice, "Calculation of muzzle blast flowfields," *AIAA Journal*, vol. 13, no. 8, pp. 1048–1055, 1975.

[2] E. M. Schmidt and D. Shear, "Optical measurements of muzzle blast," *AIAA Journal*, vol. 13, no. 8, pp. 1086–1091, 1975.

[3] E. M. Schmidt, G. D. Kahl, and D. D. Shear, "Gun blast: its propagation and determination," in *Proceedings of the 6th Aeroacoustics Conference AIAA Paper No. 80–1060*, pp. 12-13, Hartford, CT, USA, June 1980.

[4] G. Moretti, "A numerical analysis of muzzle blast precursor flow," *Computers & Fluids*, vol. 10, no. 1, pp. 51–86, 1982.

[5] G. Klingenberg, "Gun muzzle blast and flash," *Propellants, Explosives, Pyrotechnics*, vol. 14, no. 2, pp. 57–68, 1989.

[6] B.-Y Wang, "The sound source and physical characteristics of the muzzle noise," *Acta Armamentarii*, vol. 8, no. 4, pp. 1–9, 1987.

[7] Z. Jiang, K. Takayama, and B. W. Skews, "Numerical study on blast flowfields induced by supersonic projectiles discharged from shock tubes," *Physics of Fluids*, vol. 10, no. 1, pp. 277–288, 1998.

[8] X. Jiang, Z. Chen, B. Fan, and H. Li, "Numerical simulation of blast flow fields induced by a high-speed projectile," *Shock Waves*, vol. 18, no. 3, pp. 205–212, 2008.

[9] Z. Guo, Y. Wang, X. Jiang, and H. Li, "Numerical study on effects of precursor flow on muzzle propellant flow field," *Acta Armamentarii*, vol. 33, no. 6, pp. 663–668, 2012.

[10] H. Rehman, H. Chung, T. Joung, A. Suwono, and H. Jeong, "CFD analysis of sound pressure in tank gun muzzle silencer," *Journal of Central South University of Technology*, vol. 18, no. 6, pp. 2015–2020, 2011.

[11] J. Tolhurst, "Parametric design of a muzzle brake by computational fluid dynamics to reduce crew noise exposure during training," in *Proceedings of the 30th International Symposium on Ballistics*, Long Beach, CA, USA, September 2017.

[12] C. Bogey, O. Marsden, and C. Bailly, "Effects of moderate Reynolds numbers on subsonic round jets with highly disturbed nozzle-exit boundary layers," *Physics of Fluids*, vol. 24, no. 10, Article ID 105107, 2012.

[13] C. Bogey, O. Marsden, and C. Bailly, "Influence of initial turbulence level on the flow and sound fields of a subsonic jet at a diameter-based Reynolds number of 105," *Journal of Fluid Mechanics*, vol. 701, no. 6, pp. 352–385, 2012.

[14] Z.-H. Wan, L. Zhou, H.-H. Yang, and D.-J. Sun, "Large eddy simulation of flow development and noise generation of free and swirling jets," *Physics of Fluids*, vol. 25, no. 12, Article ID 126103, 2013.

[15] N. Lupoglazoff, A. Biancherin, F. Vuillot, and G. Rahier, "Comprehensive 3D unsteady simulations of subsonic and supersonic hot jet flow-fields part 1: aerodynamic analysis," in *Proceedings of the 8th AIAA/CEAS Aeroacoustics Conference & Exhibit*, June 2002.

[16] A. Biancherin, N. Lupoglazoff, G. Rahier, and F. Vuillot, "Comprehensive 3D unsteady simulations of subsonic and supersonic hot jet flow-fields part 2: acoustic analysis," in *Proceedings of the 8th AIAA/CEAS Aeroacoustics Conference & Exhibit*, June 2002.

[17] A. Sipatov, M. Usanin, and N. Chuhlantseva, "Applying fluent software for jet noise generation modeling," in *Proceedings of the 16th AIAA/CEAS Aeroacoustics Conference*, June 2010.

[18] G. A. Brès, V. Jaunet, M. L. Rallic, P. Jordan, T. Colonius, and S. K. Lele, "Large eddy simulation for jet noise: the importance of getting the boundary layer right," in *Proceedings of the 21st AIAA/CEAS Aeroacoustics Conference*, June 2015.

[19] S. A. Karabasov, M. Z. Afsar, T. P. Hynes et al., "Jet noise: acoustic analogy informed by large eddy simulation," *AIAA Journal*, vol. 48, no. 7, pp. 1312–1325, 2010.

[20] K. Viswanathan, M. B. Alkislar, and M. J. Czech, "Characteristics of the shock noise component of jet noise," *AIAA Journal*, vol. 48, no. 1, pp. 25–46, 2010.

[21] J. Bin, M. Kim, and S. Lee, "A numerical study on the generation of impulsive noise by complex flows discharging from a muzzle," *International Journal for Numerical Methods in Engineering*, vol. 75, no. 8, pp. 964–991, 2010.

[22] I. C. Lee, D.-J. Lee, S. H. Ko, D. S. Lee, and G. J. Kang, "Numerical analysis of a blast wave using CFD-CAA hybrid method," in *Proceedings of the 12th AIAA/CEAS Aeroacoustics Conference*, Cambridge, UK, May 2006.

[23] Y. Wang, X. Jiang, X. Yang et al., "Numerical simulation on jet noise induced by complex flows discharging from small caliber muzzle," *Explosion and Shock Waves*, vol. 34, no. 4, pp. 508–512, 2014.

[24] K. Lu, J. Zhao, H. Lei et al., "Distribution characteristics of muzzle noise field of high temperature and high pressure large caliber guns," *Hebei Farm Machinery*, vol. 20, no. 1, pp. 59-60, 2014.

[25] D. K. Lilly, "A proposed modification of the Germano subgrid-scale closure method," *Physics of Fluids A: Fluid Dynamics*, vol. 4, no. 3, pp. 633–635, 1992.

[26] M. Da-you, *Acoustics Manual*, Science Press, Beijing, China, 2004.

[27] B.-Y Wang, *Gun Muzzle Noise and Explosive Sound—Characteristics, Protection and Control*, National Defense Industrial Press, Beijing, China, 2001.